Visible and near infrared absorption and fluorescence studies of the adsorption and coverage of doxorubicin on single-walled carbon nanotubes

Luc Chavignon, Christophe Blanc, Tiago Serodre, May Morris, Eric Anglaret

Visible and near infrared absorption and fluorescence studies of the adsorption and coverage of doxorubicin on single-walled carbon nanotubes

Luc Chavignon[1,2]*, Christophe Blanc[1], Tiago Serodre[1], May C. Morris[2], Eric Anglaret[1]**
[1]L2C and [2]IBMM, Univ. Montpellier, CNRS, Montpellier, France

Abstract

Single-walled carbon nanotubes have been identified as promising materials for drug delivery due to their large specific surface area, their ability to pass through the cell membrane without damaging it and their physicochemical properties, allowing their surface to be easily functionalised. Additionally, their optical properties permit investigation in biological media in the near infrared (the "biological window"). In this paper, adsorption of doxorubicin on single-walled carbon nanotubes dispersed with carboxymethylcellulose salt is monitored by absorption and fluorescence spectroscopy in the visible and near infrared. We confirm that fluorescence-coupled Raman spectroscopy in the near infrared is a useful tool for probing the adsorption of drugs on single-walled carbon nanotubes in a sub-monolayer regime. By combining spectroscopic studies of doxorubicin in the visible range, we propose a protocol for quantifying the amount of adsorbed drug over a broad range of concentrations.

1. Introduction

In recent years, the intersection of nanotechnology and pharmacology has given rise to novel approaches in biosensing [1],[2],[3],[4] and drug delivery [5],[6],[7],[8]. Among the myriad of nanomaterials explored for these applications, single-walled carbon nanotubes (SWCNT) have emerged as promising candidates due to their high surface area, high aspect ratio and various physico-chemical routes for functionalizing their surface [2],[3],[4],[6],[8],[9]. Moreover, semiconducting SWCNT display exceptional optical properties including a diameter-dependent bandgap within the near infrared (NIR), associated with narrow and strong absorption and fluorescence (FL) NIR signatures in a spectral range corresponding to the « biological window » [2],[3],[4]. These optical signatures are due to excitonic transitions associated to electron-hole pairs having a diameter larger than the nanotube diameter so that the exciton binding energy,

* Corresponding author : luc.chavignon@umontpellier.fr
** Corresponding author : eric.anglaret@umontpellier.fr

and consequently the energy and intensity of the optical signatures, are very sensitive to the local dielectric environment of the nanotubes [2],[10],[11],[12]. In this context, optical spectroscopy stands out as a powerful tool for probing the intricate details of molecular adsorption at the nanoscale.

To disperse nanotubes in water and biological media for drug carrier applications, detergents and inorganic surfactants are generally avoided because of low biocompatibility and their tendency to form dense packings that cover all of the nanotube surface [13]. In contrast, natural polymers and polyelectrolytes are widely used as they can disperse nanotubes by wrapping around them, leaving large areas available at the surface of nanotubes for interactions with aromatic drug molecules via π-stacking [6],[9],[14]. Consequently, aromatic molecules can be adsorbed by simple mixing, forming "forest–scrub"-like assemblies on nanotubes with the macromolecules extending into water to impart solubility and aromatic molecules densely populating the nanotube sidewall (see *eg* [14]).

Adsorption of various drugs onto carbon nanotubes has been investigated, and primarily aromatic anti-cancer drugs, such as doxorubicin (DOX), a member of the anthracycline class of drugs which has been used widely for conventional chemotherapy since the 60s despite its toxicity [15]. DOX has been widely used as a reference drug for studies on CNT adsorption, taking advantage of its fluorescent properties, dominated by a strong FL signal around 595 nm in water [16] which allows detection in biological systems at sub-micromolar concentrations [17]. DOX adsorption onto SWCNT leads to a decrease of its absorption and FL signals. Such quenching is characteristic of π-stacking onto nanotubes [14]. Therefore, optical spectroscopy of DOX within the visible range can be used to probe adsorption onto, and release from SWCNT *in vitro* [18]. Moreover, the strong FL signal of SWCNT within NIR can be used to detect and image nanotubes both *in vitro* [19],[20] and *in vivo* [21],[22]. Furthermore, the sensitivity of NIR FL to the local dielectric environment can be used to probe the adsorption of molecular species on the nanotubes [23],[24]. In the case of drugs, the NIR FL signal of SWCNT was used to quantify exposure to doxorubicine *in vivo* [25],[26] or *in vitro* [27], with limits of detection as low as 0.1 μM [26]. However, to our best knowledge, coupling the FL signals of drugs and SWCNT to probe adsorption over a broad range of coverage has never been achieved so far.

In this paper, we present an optical spectroscopic study of the quantitative adsorption of DOX onto the surface of SWCNT dispersed with carboxymethylcellulose sodium salt (CMC). We correlate absorption and FL measurements in the visible and NIR regions to probe the stacking interactions of DOX and the local dielectric environment of SWCNT, respectively, and achieve a quantitative analysis of the adsorption and coverage of DOX on SWCNT/CMC complexes over a broad range of DOX/SWCNT mass ratio.

2. Methodology/Experimental

Purified HiPCO single-walled carbon nanotubes were purchased from NanoIntegris. Hydrochloride doxorubicin and carboxymethylcellulose sodium salt (ref C5678, M_w=90 kDa, degree of substitution -defined as the average number of sodium carboxymethyl group per anhydroglucose unit- between 0,65 and 0,9) were purchased from Sigma-Aldrich. SWCNT/CMC aqueous dispersions were prepared by mixing 20 mg of SWCNT powder and 200 mg of CMC in 20 mL of deionized water, *ie* with initial concentrations 0.1 wt% (1 g/L) SWCNT / 1 wt% (10 g/L) CMC. This mixture was tip-sonicated for 1h with duty cycles of 50% and an average power of 45 W in an ice bath to avoid overheating, and then centrifuged for 1h at a maximum acceleration of 18335 g (rotor maximum radius 7.8 cm, angle 30°, rotating speed 14500 rpm). 80% of the supernatant was collected to exclude the remaining bundles of SWCNT, then diluted 200 times. The final SWCNT concentration was determined from the measurement of the absorbance at 650 nm after centrifugation.

On the other hand, a DOX solution at 1g/L was prepared by dissolving 5 mg of DOX powder in 5 mL of deionized water, and then diluted to concentrations between 1 and 257 μM in deionized water. For concentrations above 10 μM, the DOX solutions were filtered using polycarbonate filters with 0.22 μm pores to remove DOX aggregates, which could interfere with subsequent adsorption on the nanotubes [23],[28],[29]. These DOX solutions were analyzed by UV-visible absorption spectroscopy before and after filtration to determine the absorption coefficient and the actual concentrations (see ST1 and fig. S1 in supp. Info.). Finally, 1.5 mL of some of these DOX solutions were mixed with 1.5 mL SWCNT/CMC complexes to yield samples with a constant SWCNT concentration 2.2±0.2 mg/L, and various DOX/SWCNT mass ratio, ranging from 0.1 to 30 (samples A

to K). On the other hand, an additional sample (L) was prepared with a tenfold smaller concentration of SWCNT and a DOX/SWCNT mass ratio of 100. The list of samples with their precise SWCNT and DOX concentrations is presented in Table 1.

Sample	SWCNT concentration (mg/L)	DOX concentration (μM)	DOX/SWCNT mass ratio
A	2.2 ± 0.2	1.1 ± 0.3	0.30 ± 0.11
B	2.2 ± 0.2	2.0 ± 0.3	0.49 ± 0.12
C	2.2 ± 0.2	2.1 ± 0.3	0.51 ± 0.12
D	2.2 ± 0.2	2.8 ± 0.3	0.69 ± 0.14
E	2.2 ± 0.2	4.6 ± 0.3	1.14 ± 0.18
F	2.2 ± 0.2	10.0 ± 0.5	2.47 ± 0.35
G	2.2 ± 0.2	19.9 ± 0.5	4.92 ± 0.57
H	2.2 ± 0.2	40.5 ± 0.5	10.00 ± 1.06
I	2.2 ± 0.2	59.2 ± 0.6	14.63 ± 1.48
J	2.2 ± 0.2	98.1 ± 0.6	24.24 ± 2.35
K	2.2 ± 0.2	124.9 ± 0.7	30.86 ± 2.98
L	0.22 ± 0.02	45.7 ± 0.3	112.90 ± 11.01

Table 1: *Concentrations of SWCNT in the SWCNT/CMC aqueous suspension and DOX in the aqueous solution before mixing them, and corresponding DOX/SWCNT mass ratio in the mixtures. Sample H (highlighted in orange) was selected as a reference sample throughout the paper. For samples A to E and L, the DOX concentration was calculated from the weighted mass, account for losses and incorporating error bars due to adsorption on glass surfaces. For samples F to K (grey lines) the DOX concentration was measured after filtration by UV-vis absorption spectroscopy.*

Once equilibrium was reached, after 1h as monitored spectroscopically, samples were filtered through polycarbonate filters with 0.22 μm pores to separate the SWCNT/CMC/DOX complexes from free DOX in solution. To avoid adsorption of free DOX molecules on the filter, the latter was pre-saturated with another DOX solution, at the same concentration as the filtered sample, prior to filtration. Using these precautions, we

verified that the filtration does not alter the DOX concentration. On the other hand, we confirmed that no SWCNT pass through the filter in a SWCNT/CMC dispersion although a substantial amount of free CMC -not bound to the SWNCT/CMC complexes- does. Given the easy adsorption of DOX on glass surfaces [30], only one vial and one pipette were used for each sample in order to minimize the losses and the corresponding uncertainty on the concentration. The vials were also wrapped in aluminium foil to protect DOX from the effects of light [31]. All experiments were carried out using freshly purchased DOX powder, shielded from light and stored at 5°C.

All spectroscopic measurements were performed at 22°C, using Hellma fluorescence fused quartz cuvettes thoroughly cleaned by plasma O_2 at 500 mTorr for 15 minutes between each measurement. Absorption measurements were performed with a Cary 200 Varian UV-vis-NIR absorption spectrophotometer between 380 and 1400 nm. Absorption spectra were corrected for water signal. Doxorubicin is known to self-associate in dimers within the range of concentrations studied [32],[33]. The spectral profiles of monomers and dimers display some differences, and the peak absorbance of DOX is known to be about 30% larger for monomers, dominating at low concentrations, whereas dimers are predominant at high concentrations. However, an isosbestic point exists at 540 nm, where the absorption coefficient is the same for monomers and dimers (see Supplementary text ST1). The Beer-Lamber law was therefore applied for measurements at 540 nm with a molar absorption coefficient of 4486 $L.mol^{-1}. cm^{-1}$ (fig. S1a) to determine the concentration of DOX in filtered solutions (the measured decrease in concentration due to filtration was on the order of 10%).

Doxorubicin monomers being fluorescent in aqueous solutions, measurements were also performed with a Cary Eclipse Varian fluorescence (FL) spectrophotometer between 300 and 900 nm. FL spectra of filtered DOX solutions and complexes were acquired following excitation at 490 nm. The FL spectra of DOX solutions as a function of DOX concentration are reported and commented in Supp. Info. (ST2 and fig. S2). The spectra presented hereafter were corrected for inner filter effects following the method used by Kasparek *et al.* [34].

NIR fluorescence spectra of SWCNT and complexes were measured with a Bruker RFS100 coupled Raman-FL spectrometer equipped with an Nd:YAG laser line for excitation at 1064 nm and a N_2-cooled Ge detector for acquisitions between 900 and 1700 nm.

3. Results and discussion

3.1. Absorption of DOX in the visible spectrum

Adsorption of DOX onto SWCNT was first investigated for sample H (DOX/SWCNT mass ratio approx. 10, see details in table 1) by UV-vis-NIR absorption spectroscopy between 380 and 1350 nm (figure 1). This spectral range includes the absorption range of DOX and that of SWCNT and is limited by the absorption of water above 1350 nm. The absorption spectrum of an aqueous DOX solution features a broad and intense band between 400 and 600 nm, with a peak around 480 nm, assigned to a $\pi-\pi*$ transition of the quinonoid structure, as well as a bump around 535 nm [35]. The absorption spectrum of SWCNT exhibits a series of broad, overlapping peaks in the NIR, assigned to excitonic transitions associated with the band gap of semiconducting SWCNT, with various diameters and chiral angles within HiPCO samples. As anticipated, the absorption spectrum of the mixture exhibits signatures of both materials. However, the DOX signal shows a noticeable drop and a distinct profile change, indicating adsorption of DOX molecules onto SWCNT/CMC complexes- or potentially onto free CMC. Indeed, when DOX is mixed with an aqueous solution of CMC at concentrations up to those used to prepare sample H, pronounced spectral changes are observed, reflecting intermolecular interactions, the most notable being the emergence of an additional bump around 550 nm at higher CMC concentrations (see figure S3, similar trends were also reported in reference [35] for CMC/DOX complexes prepared with comparable DOX concentrations and much higher CMC concentrations). Additionally, a systematic redshift of the SWCNT absorption peaks was observed in the NIR, as shown in the inset of fig. 1. These redshifts are indicative of structural reorganisation around the nanotubes, along with concomitant changes in their dielectric environment, further supporting the adsorption of DOX onto SWCNT/CMC complexes.

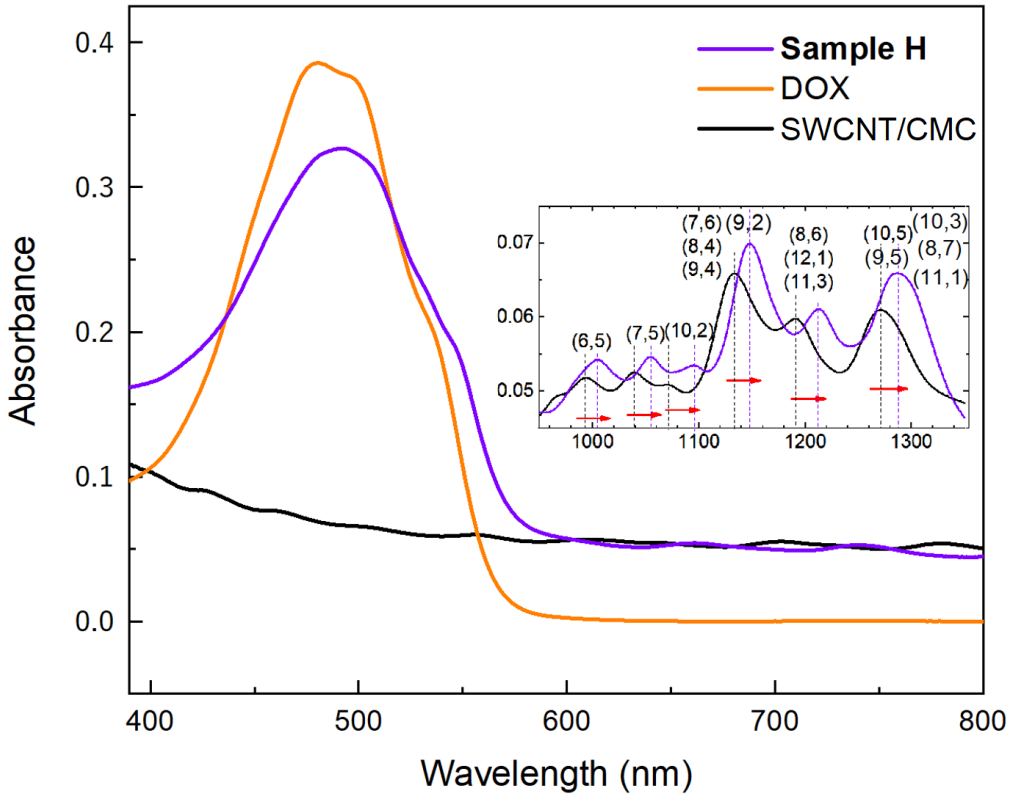

Figure 1. *Absorption spectra of sample H (purple) compared with those of its two components of same concentration: DOX solution at 40.5±0.5 μM (orange) and SWCNT/CMC complexes at 2.2±0.2 mg.L^{-1} (black). Inset: NIR part of the spectra, emphasizing the redshift of SWCNT absorption peaks, which are assigned to series of chiral indices based on typical results for HiPCO nanotubes* [36],[37].

In order to assess the respective contributions of free DOX and DOX adsorbed onto SWCNT/CMC complexes, the two fractions were separated by filtration. The absorbance of the free DOX fraction at the isosbectic point is only approximately 4 % of the initial DOX solution (fig. 2). Normalization of spectra (fig. S5) further reveals that the spectral profile of free DOX closely matches that of the initial DOX solution, notably lacking any additional bump around 550 nm. By comparing this spectral profile with those in fig. S3, one can conclude that 30% is the upper limit for passing CMC through the filter. On the other hand, it is important to consider whether the very low intensity of the free DOX signal might partially arise from adsorption onto free CMC passing through the filter. This hypothesis is excluded by the observation that DOX absorbance at the isosbestic point (540 nm) remains constant within 10% in CMC solutions, even at higher CMC

concentrations (fig. S5). Based on the calibration curve of fig. S1a, a free DOX ratio of about 4 % of the initial DOX concentration can be determined, and consequently an adsorbed DOX ratio $\phi_H \approx 0.96$. The mass ratio of adsorbed DOX to SWCNT $\left(\frac{\text{mDOX}}{\text{mSWCNT}}\right)_{\text{ads}}$ can be calculated using the following equation:

$$\left(\frac{\text{mDOX}}{\text{mSWCNT}}\right)_{\text{ads}} = \phi \left(\frac{\text{mDOX}}{\text{mSWCNT}}\right)$$

which leads to a mass ratio of about 10 for adsorbed DOX in sample H. To get more information on adsorbed DOX, its spectrum can be calculated as the difference between the spectrum of the sample and the sum of the spectra of its two components, *ie* free DOX and the SWCNT/CMC complex. The spectrum of adsorbed DOX is shifted by about 12 nm (fig. 2 and S5). This shift, assigned to intermolecular interactions within the DOX/SWCNT/CMC complexes, provides an intrinsic signature of adsorbed DOX.

In order to estimate the corresponding surface coverage, we refer to the molecular dynamics calculation of adsorption onto pristine SWCNT in an armchair conformation (7,7) by Kordzadeh *et al*, which shows that the first layer of DOX molecules stack preferentially parallel to the external surface of the SWCNT [38],[39]. Considering that the surface of the aromatic part of the DOX molecules is about 70±10 $Å^2$, and the external specific area of individual nanotubes is 1315 $m^2.g^{-1}$ [2], the order of magnitude of the DOX/SWCNT mass ratio for a compact monolayer of DOX adsorbed parallel to the external surface of individual SWCNT is estimated to about 1.7±0.2, and about the twice, 3.4±0.4 for a monolayer of dimers. These orders of magnitude do not vary significantly within the range 0.7-1.3 nm, typical of HiPCO nanotubes. On the other hand, it is important to note that this mass ratio is most likely overestimated in our samples, as the external specific surface of SWCNT decreases significantly when they are packed into small bundles, and to a lesser extent due to the partial coverage of SWCNT by CMC. On the contrary, the potential confinement of a small portion of DOX molecules inside the nanotubes would have an opposite effect [38],[39],[40]. The DOX/SWCNT mass fraction in sample H far exceeds the estimated value for a compact monolayer of dimers in a parallel configuration. This suggests that DOX molecules form a multilayered, hierarchical assembly on the SWCNT/CMC complexes, with a substantial amount likely adsorbed on the CMC, as illustrated in the right panel of figure 2. Further experimental measurements, *eg* isothermal titration calorimetry [41] or small angle neutron

scattering with isotopic labelling, and/or numerical simulations, will be required to describe more precisely the binding and organization of the DOX molecules on the SWCNT/CMC complexes in this multilayer regime.

The quenching ratio for adsorbed DOX is related to the relative decrease in absorbance at 540 nm (A_{ads}) with respect to that of the DOX component (A_{DOX}):

$$\Psi = 1 - \frac{A_{ads}}{\phi . A_{DOX}}$$

For sample H, the quenching ratio was determined to be $\psi_H \approx 0.18$.

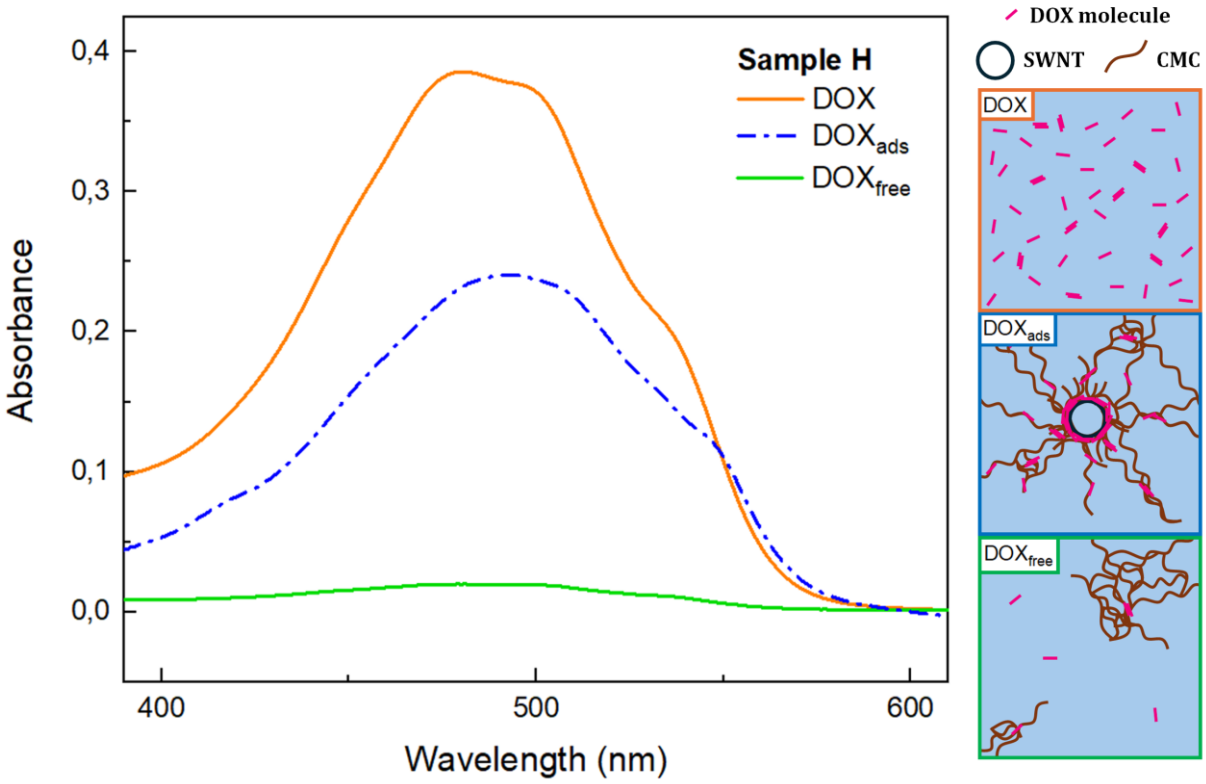

Figure 2. *Left: Absorption spectra in the spectral range of the main absorption peak of DOX for sample H: free DOX obtained by filtration (green), reference DOX solution at 40.5±0.5 μM (orange), and absorbed DOX (dot-dashed blue), calculated as the differential spectrum between that of sample H and the sum of its two components. Right: sketch of the three samples.*

To investigate whether higher concentrations of DOX can be adsorbed onto SWCNT/CMC complexes, the absorption spectrum of sample K (DOX concentration 124.9±0.5 μM, see details in table 1) is compared with the spectra of its two individual components in fig. S6a. Similar to sample H, sample K exhibits a significant decrease of the DOX signal, as well as a redshift of the SWCNT absorption peaks in the NIR region (inset of fig. S6a). After filtration, the signal of free DOX in sample K is approximately 4% of the signal of the initial DOX solution's signal (fig. S6b), comparable to sample H. The adsorbed DOX ratio for sample K, $\phi_K \approx 0.96$, translates to a mass ratio of approximately 30, nearly ninefold higher than the expected for a compact monolayer of dimers, further supporting the formation of hierarchical DOX multilayers on the SWCNT/CMC complexes. On the other hand, the relative absorbance ratio of adsorbed DOX is slightly larger than for sample H, resulting in a slightly reduced quenching ratio $\psi_K \approx 0.09$, suggesting that quenching is weaker for DOX molecules adsorbed farther from the SWCNT surface and the first adsorbed monolayer.

Finally, at lower DOX concentrations, sample F (fig. S7a and S7b) exhibits comparable qualitative and quantitative changes, though with a marginally smaller adsorbed DOX fraction, $\phi_F \approx 0.93$. This corresponds to an adsorbed DOX mass ratio of about 2.5, a value intermediate between the expected ones for compact monolayers of monomers and dimers. Notably, the quenching ratio, $\psi_F \approx 0.25$, is slightly larger than observed for higher DOX concentrations, supporting enhanced quenching efficiency for molecules or dimers within the first adsorbed monolayer.

For samples (F to K) prepared with a DOX/SWCNT ratio between 2.5 and 30, the adsorbed DOX ratio lies between 0.9 and 0.97, without any significant DOX concentration dependence, as shown in fig. 3 (data are also reported in table S1). For these series of samples, the absorption quenching ratio lies between 0.25 and 0.09, with a decreasing trend for increasing DOX concentrations (fig. 3 and table S1). These results demonstrate that large amounts of DOX can be adsorbed on SWCNT/CMC complexes, up to about 30 times the mass of the SWCNT in this study, *ie* much more than a molecular monolayer. On the other hand, the adsorbed and quenching ratio could not be measured accurately for DOX concentrations below 10 μM (*ie* DOX/SWCNT mass fractions below 2.4) because of their low absorption signals.

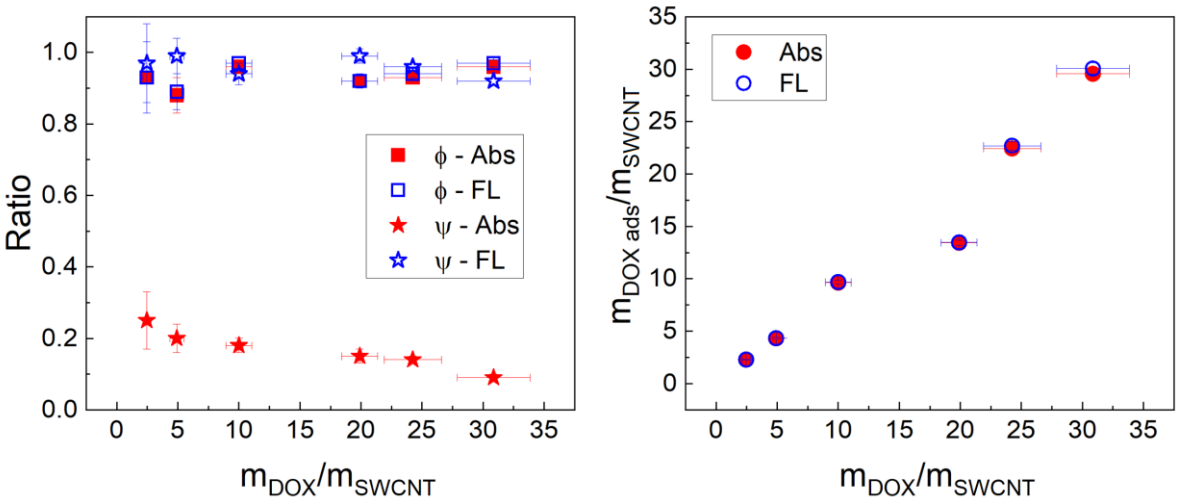

Figure 3. *Variation of the fraction of adsorbed DOX and quenching ratio (left), along with the mass ratio of adsorbed DOX to SWCNT (right), as a function of DOX/SWCNT mass ratio, as measured from visible absorption (full symbols) and fluorescence (open symbols) spectroscopies.*

3.2. Fluorescence of DOX in the visible spectral range

Adsorption of DOX on SWCNT can also be investigated by fluorescence spectroscopy in the visible. The DOX signal displays 2 maxima at 562 nm and 592 nm (the second being the most intense) and a shoulder around 638 nm, whether it is pure or mixed with SWCNT/CMC (see fig. 4 for sample H). A strong drop of intensity is observed for sample H with respect to the initial DOX solution (fig. 4). After filtration, the FL intensity of free DOX is even more reduced, to approximately 3% of the initial DOX solution's intensity. A significant decrease of intensity -though with no substantial spectral change- is also observed when DOX is mixed with an aqueous solution of CMC (fig. S4 and figure 3 in reference [35]). Given that the filtered solution contains less than 30% of the CMC used to prepare sample H, the signal from free DOX may be attenuated by adsorption onto free CMC in the filtered solution, but by no more than 25%. Therefore, the ratio of free DOX can be estimated from the calibration method described in ST2 to be about 3±1%, very close to the ratio calculated from the absorption measurements (fig. 3 and Table S1), corresponding to $\phi_{FL,H}$≈0.97±0.01. The drop in FL intensities is similar for all samples. Adsorbed DOX fractions calculated from absorption and fluorescence spectra are comparable for all samples, as shown in fig. 3 and Table S1.

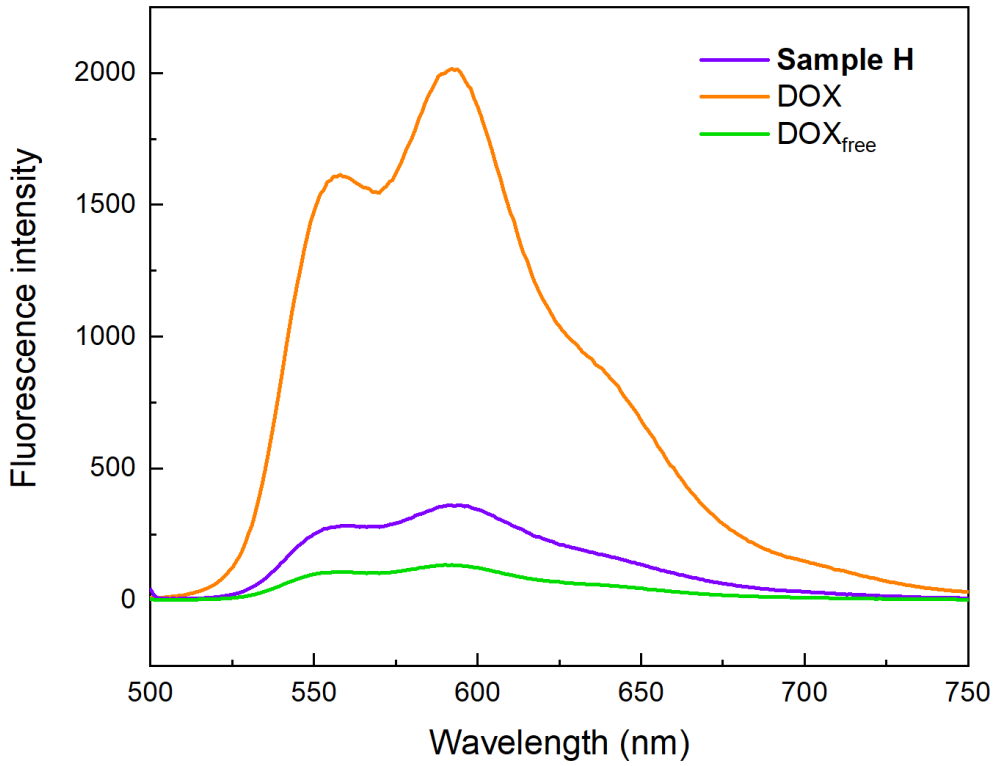

***Figure 4**: Fluorescence spectra of sample H (purple), compared to its DOX component at 40.5±0.5 μM (orange) and free DOX obtained after filtration (green)*

On the other hand, the FL quenching ratio is significantly larger than the absorption quenching ratio for all samples, between 0.92 and 0.99, indicating that FL yield is more sensitive to intramolecular interactions than the absorption transition dipole moment, as usually observed in optical spectroscopy [42]. No significant concentration dependence is observed (fig. 3).

These results show that both absorption and fluorescence of DOX in the visible spectral range are relevant approaches for monitoring and quantifying DOX adsorption onto SWCNT/CMC complexes.

3.3. NIR Raman/FL of SWCNT

Additionally, the adsorption of DOX on SWCNT can be monitored by measuring the FL signal of SWCNT in the NIR. Coupled Raman/FL spectra for sample H are shown in figure

5, featuring a dual x-axis: wavelength at the bottom and Raman shift on the top. The SWCNT/CMC spectrum displays characteristic Raman signatures of SWCNT, including a G band at 1591 cm^{-1}, a radial breathing mode (RBM) at 265 cm^{-1}, assigned to semiconducting resonant nanotubes with a diameter of about 0.9 nm. Superimposed to these narrow Raman peaks, 4 broad FL signals can be observed. The increasing FL signal at low wavelength is assigned to the resonant FL of SWCNT with chiral indices (10,2) excited with a laser energy close to their optical gap. The first FL band around 1130 nm is assigned to chiral indices (7,6), (9,4), (8,4) and (9,2) SWCNT, the second around 1200 nm to (8,6), (11,3) and (12,1) SWCNT, and the third around 1280 nm to an electron-phonon side band (EPS) of (9,5), (8,7), (10,3) and (10,5) [36],[37]. These four FL signatures are labelled in figure 5 with only the first in each series, corresponding to the largest FL intensity observed in an aqueous suspension dispersed with bile salts [36]. The strong FL intensities confirm that the nanotubes are dispersed individually or in small bundles [43]. The positions of the Raman peaks are not modified upon addition of DOX, which indicates no significant strain or doping on the SWCNT [44], and their intensities are not expected to be either. By contrast, all FL bands are significantly redshifted, similarly to what is observed in the absorption spectra (insets in fig. 1, S6a and S7a). These are the signatures corresponding to changes in the local dielectric environment of SWCNT, consequent to the adsorption of DOX onto the CMC/SWCNT complexes. Redshifts in the FL of SWCNT are typically observed when the effective dielectric constant of the surrounding environment increases, leading to dielectric screening of the Coulomb interaction and renormalization of the optical bandgap [45]. In complex DOX/CMC/water environments, numerical calculations will be necessary to better interpret the redshifts. Additionally, a notable increase in the relative intensities of the FL bands (compared to the Raman peaks) was observed, inferring that complexes undergo reorganization, thereby leading to a decreasing number of FL-quenching sites upon adsorption of DOX at their surface [43],[46]. These FL-quenching sites could include, amongst others, pockets of water [46] or interactions between nanotubes [43]. Again, numerical simulations will be needed to gain further insight into the molecular mechanisms involved.

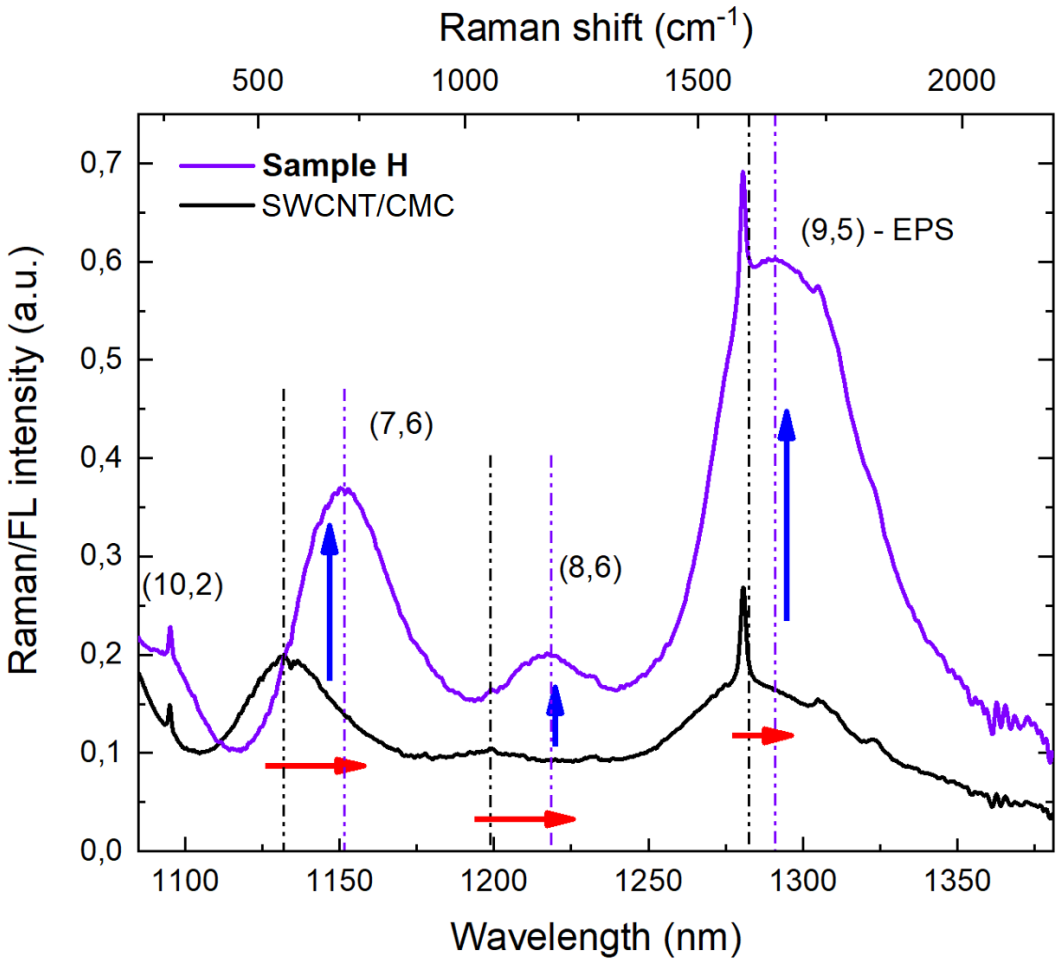

***Figure 5**: Coupled Raman/FL spectra, excited with a 1064 nm laser line, of sample H (purple) compared to the SWCNT/CMC suspension at 2.2 mg.L^{-1} (black), showing systematic redshifts and increase in FL intensities*

Similar redshifts were observed for all samples (F to L) with DOX/SWCNT mass ratio above 2.5, indicating no significant structural differences in the vicinity of the nanotube surfaces for these samples. To gain deeper insight into the effect of DOX adsorption on FL energies, it is worth studying how Raman/FL spectra are affected by smaller DOX concentrations, in a sub-monolayer regime, *ie* at mass ratio smaller than that estimated for a monolayer. The spectral features as a function of DOX/SWCNT mass ratio are displayed in fig. 6.

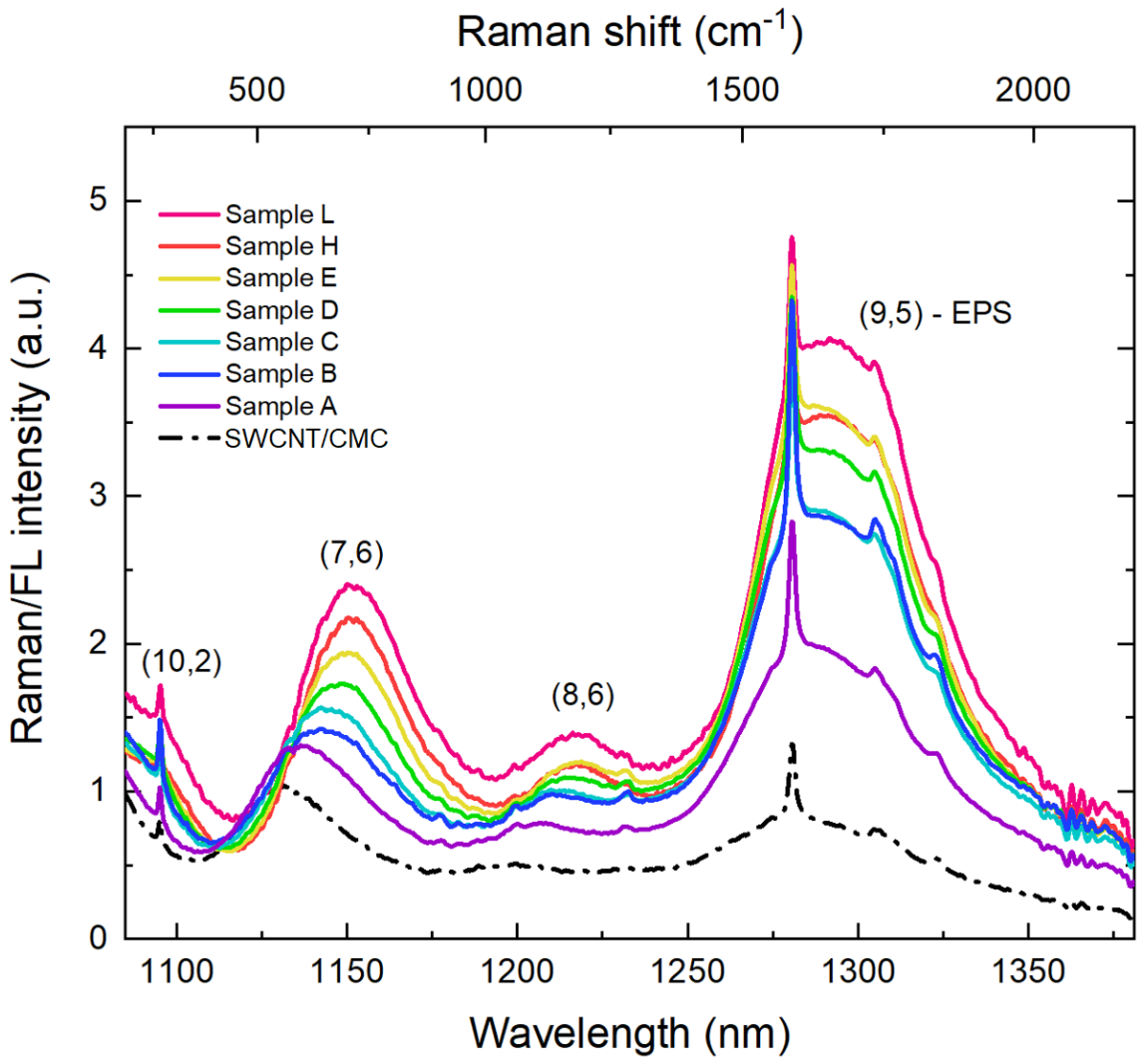

Figure 6 : *Variation of the NIR Raman/FL spectra, excited with a 1064 nm laser line, as a function of DOX/SWCNT mass ratio. Spectra are arbitrarily shifted along the y axis for clarity.*

A continuous redshift of the four main bands is observed for samples A to E, indicating a continuous change of the local dielectric environment of the nanotubes. The relative FL intensities increase continuously as well. For a more precise estimation of the shifts, each spectrum was fitted with the sum of 6 Voigt functions, *ie* 2 corresponding to the RBM and G Raman peaks, and 4 corresponding to the FL bands (the maximum of the first one, assigned to the (10,2) being not resolved. Typical fits are displayed in fig. S8 and further discussed in ST4, and the corresponding redshifts are reported in fig. 7.

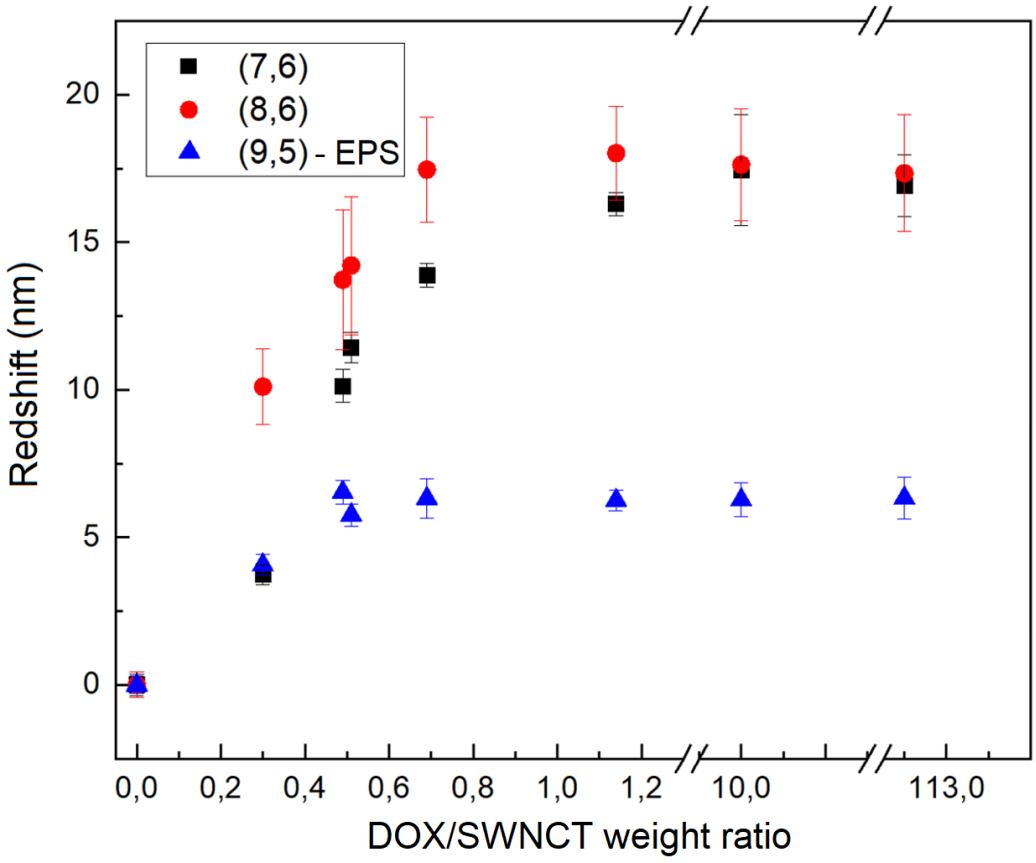

***Figure 7**: Redshift of the 3 Voigt components used to fit the 3 main FL bands of the Raman/FL NIR spectra, as a function of DOX concentration (typical fits shown in fig. S8).*

These results confirm that the three main FL bands exhibit continuous redshifts in a sub-monolayer regime, up to DOX/SWCNT mass ratio of approximately 1 (sample E). Smaller additional redshifts are observed for mass ratio about 10 (sample H) and 100 (sample L), though the latter cannot be directly compared with the others due to its preparation with a SWCNT concentration ten times smaller. This suggests that the FL wavelengths are primarily sensitive to the adsorption of the first DOX monolayer, as anticipated based on the excitons' sensitivity to the local dielectric environment. Furthermore, the redshifts of the (7,6) and (8,6) FL bands, corresponding to SWCNT diameters ranging from 0.83-0.91 nm and 0.95-1 nm, respectively, are comparable within the error margins This suggests that the local dielectric environments related to the DOX/CMC organizations at the nanotube surfaces are similar, with no strong diameter-dependence. In contrast, the redshifts are noticeably smaller for the (9,5) EPS band, which is

attributed to a different physical mechanism involving the absorption of light by a bound exciton-phonon state [36],[37],[47].

4. Conclusion

In this study, we show that the coverage rate of doxorubicin on SWCNT/CMC complexes can be quantitatively assessed by combining absorption and fluorescence spectroscopy studies of the drug and SWCNT in the visible and NIR, respectively. The adsorption ratio of DOX is high, ranging from 0.9 and 0.97, and does not exhibit any concentration dependency for DOX/SWCNT mass ratios between 2.5 and 30, making SWCNT/CMC complexes good candidates for carrying large amounts of drugs. We show that absorption and fluorescence spectra of SWCNT in the NIR are sensitive to the adsorption of DOX in the sub-monolayer regime, due to molecular reorganization around the nanotubes which modulates their local dielectric environment. These findings pave the way to further investigations to characterize kinetics of drug adsorption, coverage and release from SWCNT, whether drugs are fluorescent or not.

Acknowledgements

The authors acknowledge financial support from the LabEx NUMEV of University of Montpellier, as well as from IT Cancer of Inserm within the framework of the 2021-2030 Cancer Control Strategy, on funds administered by Inserm (TAPAS project).

References

[1] Pirzada, M. and Altintas, Z. Nanomaterials for Healthcare Biosensing Applications. *Sensors* **2019**, 19, 5311.

[2] Boghossian, A. A. , Zhang, J. , Barone, P. W. , Reuel, N. F. , Kim, J.-H. , Heller, D. A. , Ahn, J.-H. , Hilmer, A. J. , Rwei, A. , Arkalgud, J. R. , Zhang, C. T. , and Strano, M. S. Near-infrared fluorescent sensors based on single-walled carbon nanotubes for life sciences applications. *ChemSusChem* **2011**, 4, 848–863.

[3] Ferrier, D. C. and Honeychurch, K. C. Carbon Nanotube (CNT)-Based Biosensors. *Biosensors* **2021**, 11, 486.

[4] Dewey, H. M. , Lamb, A. , and Budhathoki-Uprety, J. Recent advances on applications of single-walled carbon nanotubes as cutting-edge optical nanosensors for biosensing technologies. *Nanoscale* **2024**, 16, 16344–16375.

[5] Hubbell, J. A. and Chilkoti, A. Chemistry. Nanomaterials for drug delivery. *Science (New York, N.Y.)* **2012**, 337, 303–305.

[6] Bianco, A. , Kostarelos, K. , and Prato, M. Applications of carbon nanotubes in drug delivery. *Current Opinion in Chemical Biology* **2005**, 9, 674–679.

[7] Chowdhury, D. F. Carbon Nanotube for Drug Delivery and Controlled Release☆. *In Comprehensive Biotechnology (Third Edition)*; Moo-Young, M., Ed.; Pergamon: Oxford, 2019; pp. 615–627.

[8] Zare, H. , Ahmadi, S. , Ghasemi, A. , Ghanbari, M. , Rabiee, N. , Bagherzadeh, M. , Karimi, M. , Webster, T. J. , Hamblin, M. R. , and Mostafavi, E. Carbon Nanotubes: Smart Drug/Gene Delivery Carriers. *International Journal of Nanomedicine* **2021**, 16, 1681–1706.

[9] Yang, N. , Chen, X. , Ren, T. , Zhang, P. , and Yang, D. Carbon nanotube based biosensors. *Sensors and Actuators B: Chemical* **2015**, 207, 690–715.

[10] Gao, J. , Gomulya, W. , and Loi, M. A. Effect of medium dielectric constant on the physical properties of single-walled carbon nanotubes. *Chemical Physics* **2013**, 413, 35–38.

[11] Hirana, Y. , Tanaka, Y. , Niidome, Y. , and Nakashima, N. Strong micro-dielectric environment effect on the band gaps of (n,m)single-walled carbon nanotubes. *Journal of the American Chemical Society* **2010**, 132, 13072–13077.

[12] Bergler, F. F. , Brunecker, F. K. , Hailman, M. , Schöppler, F. , and Hertel, T. Fluorescence Spectroscopy of Gel-Immobilized Single-Wall Carbon Nanotubes with Microfluidic Control of the Surfactant Environment. *The Journal of Physical Chemistry C* **2013**, 117

[13] Lin, S. and Blankschtein, D. Role of the bile salt surfactant sodium cholate in enhancing the aqueous dispersion stability of single-walled carbon nanotubes: a molecular dynamics simulation study. *The Journal of Physical Chemistry. B* **2010**, 114, 15616–15625.

[14] Liu, Z. , Sun, X. , Nakayama-Ratchford, N. , and Dai, H. Supramolecular chemistry on water-soluble carbon nanotubes for drug loading and delivery. *ACS nano* **2007**, 1, 50–56.

[15] Tacar, O. , Sriamornsak, P. , and Dass, C. R. Doxorubicin: an update on anticancer molecular action, toxicity and novel drug delivery systems. *The Journal of Pharmacy and Pharmacology* **2013**, 65, 157–170.

[16] Karukstis, K. K. , Thompson, E. H. , Whiles, J. A. , and Rosenfeld, R. J. Deciphering the fluorescence signature of daunomycin and doxorubicin. *Biophysical Chemistry* **1998**, 73, 249–263.

[17] Kauffman, M. K. , Kauffman, M. E. , Zhu, H. , Jia, Z. , and Li, Y. R. Fluorescence-Based Assays for Measuring Doxorubicin in Biological Systems. *Reactive Oxygen Species (Apex, N.C.)* **2016**, 2, 432–439.

[18] Liu, Z. , Fan, A. C. , Rakhra, K. , Sherlock, S. , Goodwin, A. , Chen, X. , Yang, Q. , Felsher, D. W. , and Dai, H. Supramolecular stacking of doxorubicin on carbon nanotubes for in vivo cancer therapy. *Angewandte Chemie (International Ed. in English)* **2009**, 48, 7668–7672.

[19] Welsher, K. , Liu, Z. , Daranciang, D. , and Dai, H. Selective probing and imaging of cells with single walled carbon nanotubes as near-infrared fluorescent molecules. *Nano Letters* **2008**, 8, 586–590.

[20] Welsher, K. , Liu, Z. , Sherlock, S. P. , Robinson, J. T. , Chen, Z. , Daranciang, D. , and Dai, H. A route to brightly fluorescent carbon nanotubes for near-infrared imaging in mice. *Nature Nanotechnology* **2009**, 4, 773–780.

[21] Liu, Z. , Tabakman, S. , Welsher, K. , and Dai, H. Carbon Nanotubes in Biology and Medicine: In vitro and in vivo Detection, Imaging and Drug Delivery. *Nano Research* **2009**, 2, 85–120.

[22] Barone, P. W. , Parker, R. S. , and Strano, M. S. In vivo fluorescence detection of glucose using a single-walled carbon nanotube optical sensor: design, fluorophore properties, advantages, and disadvantages. *Analytical Chemistry* **2005**, 77, 7556–7562.

[23] Barone, P. W. , Baik, S. , Heller, D. A. , and Strano, M. S. Near-infrared optical sensors based on single-walled carbon nanotubes. *Nature Materials* **2005**, 4, 86–92.

[24] Nißler, R. , Mann, F. A. , Chaturvedi, P. , Horlebein, J. , Meyer, D. , Vuković, L. , and Kruss, S. Quantification of the Number of Adsorbed DNA Molecules on Single-Walled Carbon Nanotubes. **2019**

[25] Harvey, J. D. , Williams, R. M. , Tully, K. M. , Baker, H. A. , Shamay, Y. , and Heller, D. A. An in Vivo Nanosensor Measures Compartmental Doxorubicin Exposure. *Nano Letters* **2019**, 19, 4343–4354.

[26] Cohen, Z. , Alpert, D. J. , Weisel, A. C. , Ryan, A. , Roach, A. , Rahman, S. , Gaikwad, P. V. , Nicoll, S. B. , and Williams, R. M. Noninvasive Injectable Optical Nanosensor-Hydrogel Hybrids Detect Doxorubicin in Living Mice. *Advanced Optical Materials* **2024**, 12, 2303324.

[27] Del Bonis-O'Donnell, J. T. , Pinals, R. L. , Jeong, S. , Thakrar, A. , Wolfinger, R. D. , and Landry, M. P. Chemometric Approaches for Developing Infrared Nanosensors To Image Anthracyclines. *Biochemistry* **2019**, 58, 54–64.

[28] Fülöp, Z. , Gref, R. , and Loftsson, T. A permeation method for detection of self-aggregation of doxorubicin in aqueous environment. *International Journal of Pharmaceutics* **2013**, 454, 559–561.

[29] Yamada, Y. Dimerization of Doxorubicin Causes Its Precipitation. *ACS omega* **2020**, 5, 33235–33241.

[30] Wu, D. C. and Ofner, C. M. Adsorption and degradation of doxorubicin from aqueous solution in polypropylene containers. *AAPS PharmSciTech* **2013**, 14, 74–77.

[31] Wood, M. J. , Irwin, W. J. , and Scott, D. K. Photodegradation of doxorubicin, daunorubicin and epirubicin measured by high-performance liquid chromatography. *Journal of Clinical Pharmacy and Therapeutics* **1990**, 15, 291–300.

[32] Menozzi, M. , Valentini, L. , Vannini, E. , and Arcamone, F. Self-association of doxorubicin and related compounds in aqueous solution. *Journal of Pharmaceutical Sciences* **1984**, 73, 766–770.

[33] Changenet-Barret, P. , Gustavsson, T. , Markovitsi, D. , Manet, I. , and Monti, S. Unravelling molecular mechanisms in the fluorescence spectra of doxorubicin in aqueous solution by femtosecond fluorescence spectroscopy. *Physical Chemistry Chemical Physics* **2013**, 15, 2937–2944.

[34] Kasparek, A. and Smyk, B. A new approach to the old problem: Inner filter effect type I and II in fluorescence. *Spectrochimica Acta. Part A, Molecular and Biomolecular Spectroscopy* **2018**, 198, 297–303.

[35] Carvalho, S. M. , Mansur, A. A. P. , Capanema, N. S. V. , Carvalho, I. C. , Chagas, P. , Oliveira, L. C. A. de , and Mansur, H. S. Synthesis and *in vitro* assessment of anticancer hydrogels composed by carboxymethylcellulose-doxorubicin as potential transdermal delivery systems for treatment of skin cancer. *Journal of Molecular Liquids* **2018**, 266, 425–440.

[36] Pfohl, M. , Tune, D. D. , Graf, A. , Zaumseil, J. , Krupke, R. , and Flavel, B. S. Fitting Single-Walled Carbon Nanotube Optical Spectra. *ACS omega* **2017**, 2, 1163–1171.

[37] Torres-Canas, F. J. Tintas y materiales compuestos anisotrópicos basados en nanotubos de carbono.

[38] Kordzadeh, A. , Amjad-Iranagh, S. , Zarif, M. , and Modarress, H. Adsorption and encapsulation of the drug doxorubicin on covalent functionalized carbon nanotubes: A scrutinized study by using molecular dynamics simulation and quantum mechanics calculation. *Journal of Molecular Graphics & Modelling* **2019**, 88, 11–22.

[39] Wang, C. , Zhang, L. , Jiang, Y. , Zhang, M. , Liu, L. , Ye, D. , Zhang, S. , and Yang, Y. A DFT study on the high-density assembly of doxorubicin drug delivery by single-walled carbon nanotubes. *Physica E: Low-dimensional Systems and Nanostructures* **2021**, 134, 114892.

[40] Contreras, L. , Villarroel, I. , Torres, C. , and Rozas, R. Doxorubicin Encapsulation in Carbon Nanotubes Having Haeckelite or Stone-Wales Defects as Drug Carriers: A Molecular Dynamics Approach. *Molecules (Basel, Switzerland)* **2021**, 26, 1586.

[41] Waters, L. J. , Swaine, T. S. , and Lewis, A. L. A calorimetric investigation of doxorubicin-polymer bead interactions. *International Journal of Pharmaceutics* **2015**, 493, 129–133.

[42] Molecular Fluorescence: Principles and Applications, 2nd Edition | Wiley. https://www.wiley.com/en-us/Molecular+Fluorescence%3A+Principles+and+Applications%2C+2nd+Edition-p-9783527650026 (accessed May 28, 2025).

[43] O'Connell, M. J. , Bachilo, S. M. , Huffman, C. B. , Moore, V. C. , Strano, M. S. , Haroz, E. H. , Rialon, K. L. , Boul, P. J. , Noon, W. H. , Kittrell, C. , Ma, J. , Hauge, R. H. , Weisman, R. B. , and Smalley, R. E. Band gap fluorescence from individual single-walled carbon nanotubes. *Science (New York, N.Y.)* **2002**, 297, 593–596.

[44] Jorio, A. and Saito, R. Raman spectroscopy for carbon nanotube applications. *Journal of Applied Physics* **2021**, 129, 021102.

[45] Ohno, Y. , Iwasaki, S. , Murakami, Y. , Kishimoto, S. , Maruyama, S. , and Mizutani, T. Excitonic transition energies in single-walled carbon nanotubes: Dependence on environmental dielectric constant. *physica status solidi (b)* **2007**, 244, 4002–4005.

[46] Duque, J. G. , Oudjedi, L. , Crochet, J. J. , Tretiak, S. , Lounis, B. , Doorn, S. K. , and Cognet, L. Mechanism of Electrolyte-Induced Brightening in Single-Wall Carbon Nanotubes. *Journal of the American Chemical Society* **2013**, 135, 3379–3382.

[47] Perebeinos, V. , Tersoff, J. , and Avouris, P. Effect of Exciton-Phonon Coupling in the Calculated Optical Absorption of Carbon Nanotubes. *Physical Review Letters* **2005**, 94, 027402.